Biaxially Stretchable, Integrated Array of High Performance Microsupercapacitors

By Yein Lim,[†] Jangyeol Yoon,[‡] Junyeong Yun,[‡] Daeil Kim,[‡] Soo Yeong Hong,[‡] Seung-Jung Lee,[§] Goangseup Zi,[§] and Jeong Sook Ha*[,†,‡]

[†]KU-KIST Graduate School of Converging Science and Technology, Korea University, Seoul 136-701, Republic of Korea, [‡]Department of Chemical and Biological Engineering, Korea University, Seoul 136-701, Republic of Korea, and [§]Department of Civil, Environmental and Architectural Engineering, Korea University, Seoul 136-701, Republic of Korea

ABSTRACT We report on the fabrication of a biaxially stretchable array of high performance microsupercapacitors (MSCs) on a deformable substrate. The deformable substrate is designed to suppress local strain applied to active devices by locally implanting pieces of stiff polyethylene terephthalate (PET) films within the soft elastomer of Ecoflex. A strain suppressed region is formed on the top surface of the deformable substrate, below which PET films are implanted. Active devices placed within this region can be isolated from the strain. Analysis of strain distribution by finite element method confirms that the maximum strain applied to MSC in the strain suppressed region is smaller than 0.02%, while that on the Ecoflex film is larger than 250% under both uniaxial strain of 70% and biaxial strain of 50%. The all-solid-state planar MSCs, fabricated with layer-by-layer deposited multiwalled carbon nanotube electrodes and patterned ionogel electrolyte of poly(ethylene glycol) diacrylate and 1-ethyl-3-methylimidazolium bis(trifluoromethylsulfonyl)imide having high-potential windows, are dry-transferred onto the deformable substrate and electrically connected in series and parallel *via* embedded liquid metal interconnection and Ag nanowire contacts. Liquid metal interconnection, formed by injecting liquid metal into the microchannel embedded within the substrate, can endure severe strains and requires no additional encapsulation process. This formed MSC array exhibits high energy and power density of 25 mWh/cm^3 and 32 W/cm^3, and stable electrochemical performance up to 100% uniaxial and 50% biaxial stretching. The high output voltage of the MSC array is used to light micro-light-emitting diode (μ-LED) arrays, even under strain conditions. This work demonstrates the potential application of our stretchable MSC arrays to wearable and bioimplantable electronics with a self-powered system.

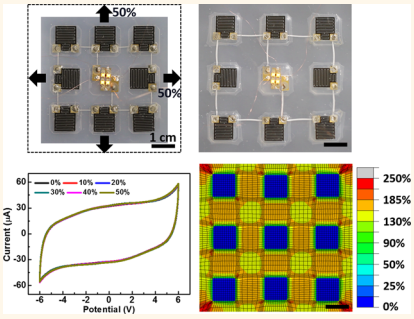

KEYWORDS: biaxially stretchable · all-solid-state microsupercapacitor array · patternable ionogel electrolyte · high power and energy density · liquid metal interconnection

According to the increasing demand for wearable and bioimplantable applications, various devices are required to be flexible and stretchable for conforming to noncoplanar surfaces, including the human body.[1] Stretchable electronics are designed to operate with no mechanical or electrical degradation under various strain conditions: twisting, bending, folding, and stretching.[2] Thus, they have potential applications as portable, wearable, and bioimplantable devices.

Until now, there has been extensive research on stretchable electronic devices so that various types of devices have been developed, such as light-emitting diodes (LEDs),[3] display panels,[4] radio frequency (RF) electronics,[5] strain and pressure sensors,[6] transistors,[7] and epidermal electronics.[8] Furthermore, these active devices should be integrated with energy storage devices to organize independent, self-powered systems; otherwise, they will require power to be supplied from an external source with wire connections.

Among energy storage devices, supercapacitors exhibit many advantages, including rapid charge/discharge rates, high power density, long cycle life, relatively simple design, and safety.[9−11] There are two types of supercapacitors, depending on the charging principles: electrical double layer capacitor (EDLC) and redox supercapacitor.[12,13] An EDLC can be easily assembled into an all-solid-state power source, which is sufficiently light and flexible to be applied in portable devices.[14] Carbon based materials, including activated

* Address correspondence to jeongsha@korea.ac.kr.

Received for review September 2, 2014 and accepted October 27, 2014.

Published online October 27, 2014
10.1021/nn504925s

carbon, carbon nanotube (CNT), and graphene, are primarily used as electrodes for EDLC due to their high electrical conductivity, large specific surface area, and chemical stability.[15,16]

In accordance with the development of stretchable electronics applied to wearable or body-implanted devices, there have been enormous efforts toward the fabrication of supercapacitors in stretchable form. Two strategies have been adopted to fabricate stretchable supercapacitors: (1) designing novel device structures and (2) utilizing the elastic property of the material.[17] Supercapacitors using rigid (carbon and metal based) materials with buckled structures,[18,19] serpentine interconnections,[20] and textiles[21] used the novel design concept. Energy devices based on a stretchable matrix with conductive polymer are included in the strategy of utilizing the material properties.[22] In a conventionally configured supercapacitor (two electrodes, separator, and liquid electrolyte), the electrolyte may leak and there may be relative displacement among the configuration components, which decreases device performance during stretching.[23,24] Supercapacitor with a buckled structure is difficult to integrate into circuitry. However, all-solid-state planar type supercapacitors can solve above-mentioned problems and are suitable for integration into stretchable electronic circuits. Additionally, they can be fabricated sufficiently thinly to not require a separator and to reduce the ion travel path.[25,26]

In our previous work, all-solid-state microsupercapacitors (MSCs) were integrated with serpentine interconnections to be a stretchable supercapacitor array.[20] In this case, however, the process is complicated, and the interconnection is vulnerable to external impact. In addition, repetitive stretching cycles degrade the performance of the MSC array due to the surface covered ion-gel electrolyte, restricting the pop-up of the serpentine interconnections.

In this study, we report on the fabrication of a high-performance biaxially stretchable all-solid-state MSC array. The all-solid-state MSC is composed of a layer-by-layer (LbL) assembled thin film of MWNTs on Au electrodes and a patterned ionogel electrolyte that exhibits a broad operation voltage window, resulting in both high energy and power density, and stability under repeated deformation.

To achieve superior stretchability, we adopted a novel structure for the deformable substrate and used its intrinsic properties of interconnection instead of making the MSC stretchable. Within the soft elastomer (Ecoflex) substrate, the relatively stiffer material of polyethylene terephthalate (PET) film was locally implanted. On the top surface of the substrate below which the PET film is implanted, a strain suppressed zone is formed. By placing the MSCs in the zone, the devices can be isolated from the strains. The embedded microchannels are filled with liquid metal alloy to form electrical interconnections between the individual MSCs. This liquid metal interconnection can endure severe strains without additional encapsulation processes. Despite these many advantages of liquid metal interconnection, technical improvement in fabricating interconnection with liquid metal may be needed for its broader application as practical technology comparable to the serpentine interconnections.[20] Recently reported works suggest various new ways of liquid metal patterning.[27−31]

Such formed MSC array exhibited high performance without degradation at up to 100% uniaxial and 50% biaxial stretching. By creating the integrated circuit of MSCs, the output voltage and capacitance were controlled as required. The high output voltage of MSC array was used to light μ-LED arrays under strain.

Compared to our recent work,[32] this work suggests a novel stretchable MSC array expected to be applied in the wider range of future wearable and bioimplanted devices owing to its smaller thickness and flat surface. The local strain applied to the MSC region can be more efficiently suppressed by strain minimizing design with stiff PET film locally implanted in the soft Ecoflex substrate so that the stretchability is greatly increased both in uniaxial and biaxial directions. Besides, the fabrication process is much simplified due to the planar arrangement of liquid metal interconnections. The performance of MSC, in terms of output voltage, energy density and power density, is highly improved while enhanced stability is achieved. The use of patterned solid film of electrolyte also makes the facile integration of the MSC onto the deformable substrate.

The results of this work demonstrate the potential application of our biaxially stretchable MSC arrays for wearable and bioimplantable devices with self-powered systems.

RESULTS AND DISCUSSION

Figure 1 demonstrates the primary design concept for a stretchable MSC array on a deformable substrate. To fabricate the stretchable MSC array, we adopted four strategies in terms of structure, material, and process, as discussed in the following.

(1) Soft elastomer substrate with implanted PET films: To minimize the local strain applied to the active devices, we adopted a deformable substrate composed of a soft elastomer substrate, Ecoflex (modulus: 69 kPa),[33] with implanted PET films. On the local area of the substrate below which the stiffer PET (modulus: 2.0−2.7 GPa)[34] films are implanted, a strain suppressed region is formed. The MSCs attached on this region can be isolated from the strains even if the whole device is under severe strain conditions. In addition, the adhesion between the active devices and the top surface of the deformable substrate can be enhanced by such implanted PET films, resulting in the enhanced strength over repeated deformation.

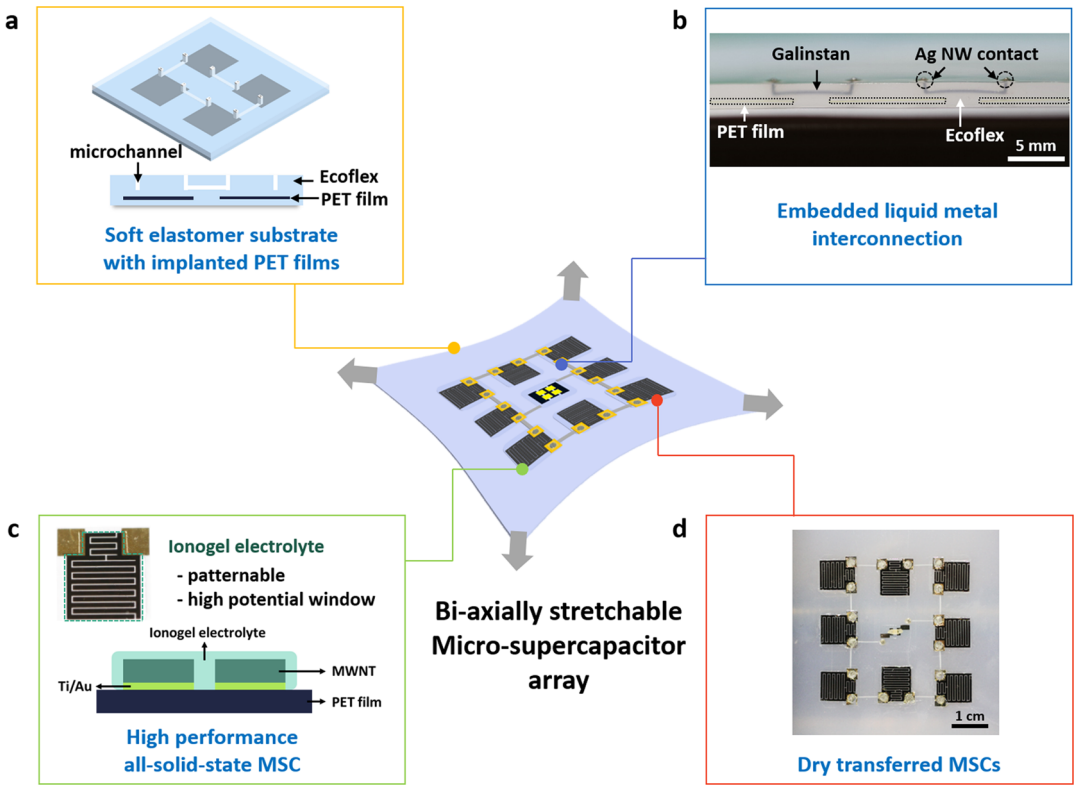

Figure 1. Primary design concept of biaxially stretchable MSC array on a deformable substrate. (a) Structure of the deformable substrate, composed of Ecoflex with implanted PET films and embedded microchannel for liquid metal interconnection. (b) Cross-sectional image of liquid metal interconnection embedded within the substrate and sealed with Ag NW contact. (c) Optical image (top) and cross-sectional scheme (bottom) of the high-performance all-solid-state MSC with ionogel electrolyte. (d) MSC array attached on the deformable substrate *via* dry-transfer method.

(2) Embedded liquid metal interconnection: Liquid metal Galinstan shows high electrical conductivity of 3.46×10^6 S/m and forms a stable microstructure in the microchannel, which is used as an electrical interconnection between the individual MSCs.[35,36] The liquid metal interconnection is formed by using a microsyringe to simply inject liquid metal alloy into the microchannel embedded within the substrate. This interconnection is safe from external impact with no additional encapsulation process and can endure a highly stretched state. The liquid metal interconnection and Au pad of the MSC are electrically connected by Ag nanowire (NW) contact. Ag NW percolation can electrically connect MSC with the liquid metal and provide a stable sealing of embedded liquid metal. To prove the stability of liquid metal interconnection, an electrical measurement was conducted through such electrical connections with repetitive uniaxial strain of 70% as shown in Figure S1. Schematic diagram of deformable substrate with liquid metal interconnection and Ag NW contact is shown in Figure S1a. No noticeable change in the electrical performance was exhibited under 10 000 times of mechanical cycles for 11 h as shown in Figure S1b. By using embedded liquid metal interconnection, the fill factor can be increased significantly compared to that obtained by using suspended serpentine interconnection in our previous work.[20] The suspended serpentine interconnection requires the considerably large spacing between the active devices for relieving the strain.

(3) High performance all-solid-state MSC: The fabricated all-solid-state MSC is composed of interdigitated MWNT/Au electrodes fabricated by using layer-by-layer deposition of MWNTs and patterned ionogel electrolyte with higher potential window (from -1.5 to $+1.5$ V) than conventionally used electrolyte of PVA/H_3PO_4 (from 0 to 0.8 V); thus, the MSC shows reproducible and high performance under ambient conditions. The interspace between interdigitated electrodes is patterned at 150 μm.

(4) Dry-transferred MSC: The MSCs are fabricated on the PET substrate attached on the polydimethylsiloxane (PDMS) coated Si/SiO_2 and dry-transferred to the deformable substrate. The processes for the fabrication of substrate and devices can be conducted independently so that different types of devices can be applied to the substrate and the design of the substrate is variable.

The whole fabrication process consists of three steps: fabrication of stretchable substrate, fabrication of all-solid-state MSCs, and integration of the MSCs on the stretchable substrate. The deformable substrate with multilayered structure was fabricated by molding

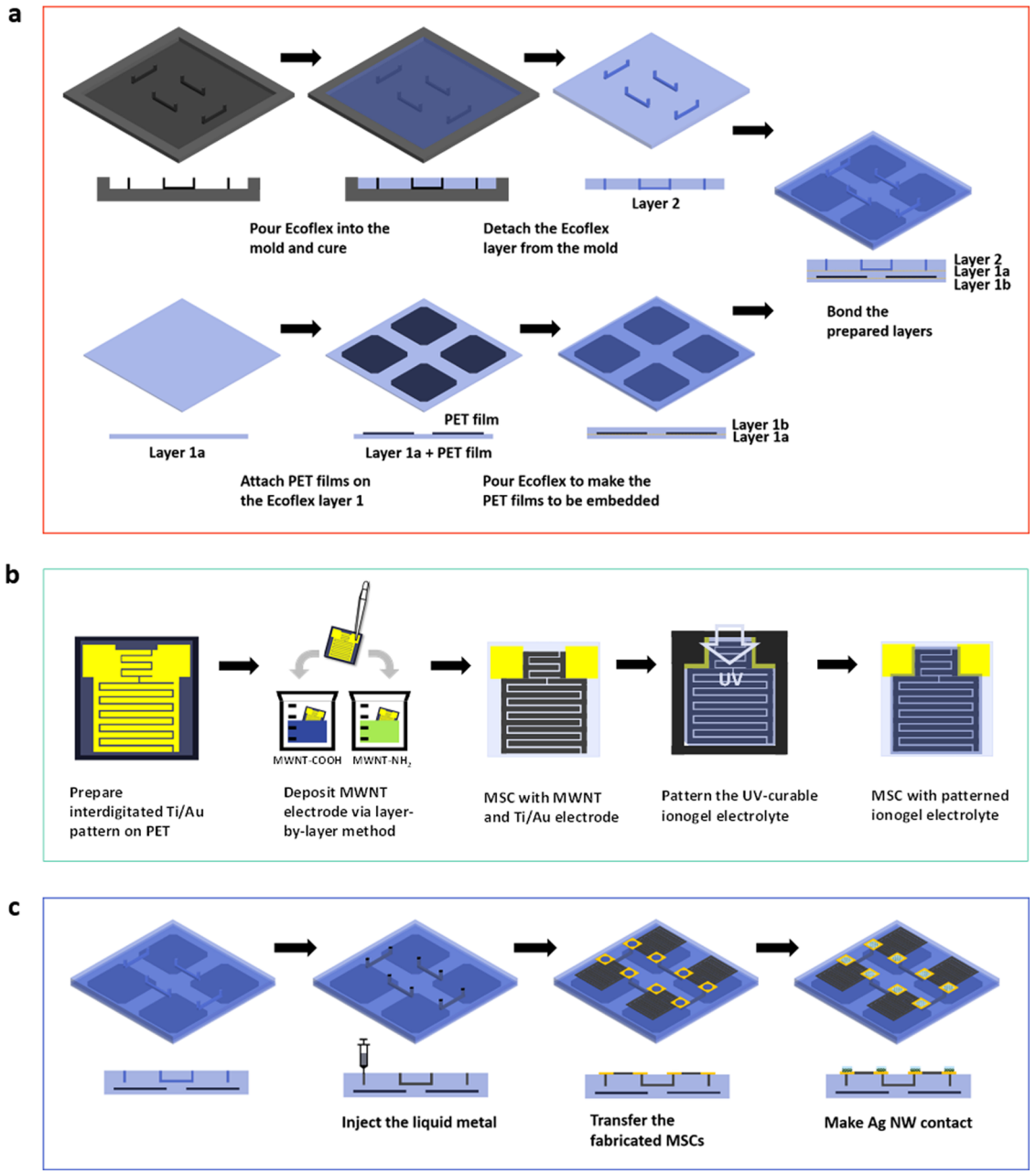

Figure 2. Schematic illustration of the fabrication process for the stretchable MSC array on a deformable substrate. Fabrication of (a) the deformable substrate and (b) high-performance MSC with patterned ionogel electrolyte. (c) Integration of the fabricated MSCs on the deformable substrate *via* liquid metal injection, dry-transfer process, and formation of electrical contact with Ag NWs.

several elastomer layers and assembling them together, as shown in Figure 2a.

A mixture of Ecoflex prepolymer and curing agent (Ecoflex 0030, Smooth-On) was prepared with a weight mixing ratio of 1:1. The mixture was poured into the mold with thin wires protruding from the flat bottom surface. The Ecoflex mixture in the mold was annealed in an oven at 65 °C for 30 min. Next, the cured top Ecoflex layer was detached from the mold, and open microchannels were shown on the underside of the layer (layer 2).

The middle layer of Ecoflex, 0.3 mm thick, was made by molding (layer 1a). Above layer 1a, nine pieces of square PET films (11 mm × 11 mm × 0.1 mm) were attached by using a small amount of uncured Ecoflex. The four corners of square PET films were cut off to avoid high strains around the sharp corners. The adjacent PET films were 4 mm apart. Uncured Ecoflex was poured onto this layer to make a 0.5 mm-thick bottom Ecoflex layer (layer 1b). Consequently, the PET films were embedded within the 0.8 mm-thick Ecoflex layer. The resulting layer was inverted. Next, on the surface, thin Ecoflex layer was spin-coated at 2000 rpm for 50 s and cured at 60 °C for 1 min to be used as a bonding layer between layers 1a and 2. The whole

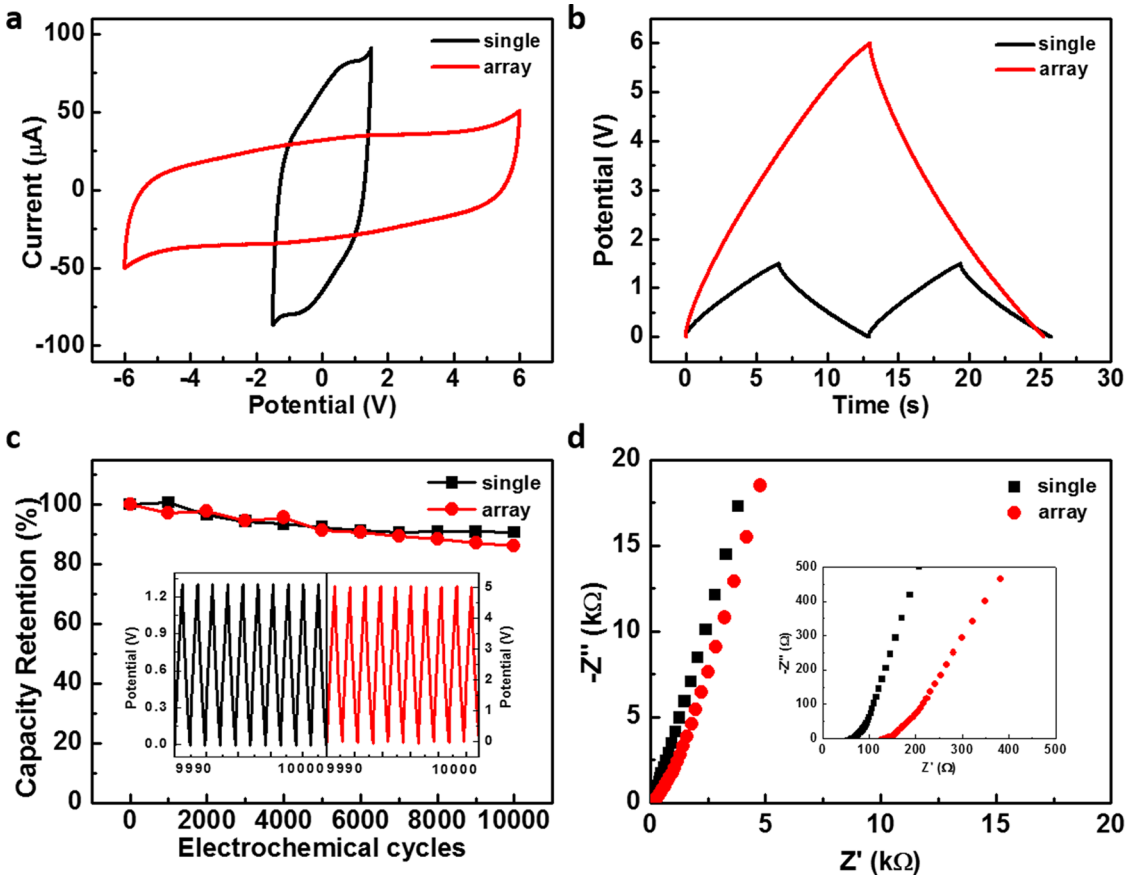

Figure 3. Electrochemical performance of single MSC (black) and MSC array (red) with LbL deposited MWNT electrodes in ionogel electrolyte. (a) CV measurements at scan rate of 1 V/s. (b) Galvanostatic charge/discharge curves at current of 13.2 μA. (c) Capacity retention of single MSC and MSC array with 10 000 charge/discharge cycles at a current of 30 μA. The inset shows the charge/discharge curves observed at the repetition between 9990 and 10 000. (d) Nyquist impedance plot of single MSC and MSC array at frequency ranging from 500 kHz to 0.1 Hz. ESR values are 66 and 133 Ω for single MSC and MSC array, respectively.

assembled substrate was cured completely in the oven.

The fabrication process of the all-solid-state MSC is demonstrated in Figure 2b. Patterned Ti/Au electrodes were prepared on the PET substrate by photolithography and e-beam evaporation. The functionalized MWNT film was deposited on the Ti/Au electrode *via* LbL assembly: The Ti/Au electrodes were alternately dipped into MWNT-COOH and MWNT-NH_2 dispersion solutions for 10 min each and rinsed thoroughly with deionized (DI) water. This cycle was repeated 10 times to get 10 bilayer MWNT thin films. The thickness of LbL deposited MWNT film was controlled by adjusting the number of LbL cycles, resulting in the reproducible performance of multiple MSCs. A scanning electron microscopy (SEM) image of the fabricated MSC electrode is shown in Supporting Information Figure S2. This figure shows the percolated MWNTs (Supporting Information Figure S2a); the thickness of the MWNT film is estimated to be 250 nm according to the cross-sectional image (Supporting Information Figure S2b).

Ionogel electrolyte, composed of poly(ethylene glycol) diacrylate and 1-ethyl-3-methylimidazolium bis(trifluoromethylsulfonyl)imide (PEGDA/[EMIM][TFSI]), was drop-cast onto the MWNT/Au electrodes and ultraviolet (UV) light was irradiated through a shadow mask. The unexposed part of the ionogel was removed by dipping it in chloroform for 5 s, gently rinsing with DI water, and blowing with N_2 gas. A *via* hole with diameter of 2 mm was punched on the Au pad of the fabricated MSC to connect the liquid metal interconnection with the MSC. Eight differently fabricated MSCs exhibited capacitance variation within 8%, which indicates that the individual MSCs were fabricated with almost the same performance (Supporting Information Figure S2c).

In Figure 2c, the liquid metal Galinstan was injected into the embedded microchannel of the previously fabricated elastomeric substrate with implanted PET films. Eight MSCs were dry-transferred onto the substrate. For the electrical connection between MSCs and interconnections, Ag NW contact was made by repeatedly dropping and drying the Ag NW dispersion solution. Next, a small amount of PDMS was pasted onto the Ag NW contact for further protection.

The electrochemical performances of the single MSC and the MSC array with LbL deposited MWNT and ionogel electrolyte were compared. In this case, the MSC array consists of a pair of parallel connected MSC arrays of four

serially connected MSCs, 2P + 4S, as shown in Supporting Information Figure S3. Fill factor is defined by the relation, fill factor = active area of MSC/total area including MSC and the interconnections. In our previous work on stretchable MSCs using serpentine interconnections,[20] the active area of MSC and the total area were 0.0172 and 0.126 cm^2, respectively. Thus, the fill factor was estimated to be 13.6%. In this work, the active area of MSC is 0.66 cm^2 and the total area is 1.87 cm^2, estimating the fill factor to be 35.3%. By adopting the embedded interconnection, the fill factor can be increased more than double.

Cyclic voltammetry (CV) curves taken from a single MSC and an MSC array at a scan rate of 1 V/s are shown in Figure 3a. The voltage windows for the single MSC and the MSC array connected in 2P + 4S range from −1.5 to 1.5 V and −6 to 6 V, respectively. The CV curves formed rectangular shapes, which implies fast ion diffusion and efficient electrical double layer (EDL) formation for ideal capacitive behavior.[37−39] The total capacitance can be calculated from the area of the CV curves by using the following eq 1:

$$C_T = \frac{\int I\,dV}{\Delta V \cdot S} \quad (1)$$

where I, ΔV, and S are the discharge current, operation voltage window, and scan rate, respectively.[39] On the basis of this equation, the calculated total capacitance values for single MSC and MSC array are 54.5 and 27.3 μF. When the MSCs are connected with four series and two parallel, the voltage window shows a quadruple increase, and the total capacitance of the MSC array should be half the total capacitance of a single MSC. Thus, the calculated capacitance corresponds to the expected value, which indicates that the eight MSCs were successfully integrated into a circuit through the liquid metal interconnections and Ag NW contacts. The volumetric capacitance values are estimated to be 13.2 F/cm^3 and 0.826 F/cm^3 for single MSC and MSC array, respectively. Here, the total area including interdigitated electrodes and interspaces (150 μm) is calculated to be 0.66 cm^2 as shown in Supporting Information Figure S4, and the thickness of the electrode is 250 nm.

Figure 3b shows galvanostatic charge/discharge curves of the single MSC and MSC array at a current of 13.2 μA. Both curves show linear and nearly triangular shape, which signifies capacitive behavior with less faradic reaction.[40,41] The times for one charge/discharge cycle are 13 and 25 s for single MSC and MSC array, respectively. The discharging time for the MSC array is two times longer than that for single MSC, which also agrees reasonably with the expected results for a 2P + 4S connection. Coulombic efficiency was calculated by using the equation below.

$$\eta\,(\%) = \frac{t_D}{t_C} \times 100 \quad (2)$$

where t_D and t_C are the discharging time and charging time, respectively. The Coulombic efficiency values were estimated to be 97 and 94% for single device and array, respectively, which indicates remarkable reversibility of the charge/discharge processes. According to the charge/discharge curves, voltage drops were derived to be 0.052 and 0.089 V for single device and array, respectively. As with the single MSC, the MSC array exhibited a small voltage drop, implying that it still retains low internal resistance.[42,43] In other words, MSCs are connected into an array without energy loss. CV curves at various scan rates and galvanostatic charge/discharge curves at various currents are shown in Supporting Information Figure S5.

Figure 3c shows the capacity retention of single MSC and MSC array, taken with 10 000 charge/discharge cycles at a current of 30 μA. Even after 10 000 galvanostatic charge/discharge cycles, the triangular shape of the curves is maintained. Additionally, 91 and 86% of initial capacitance were retained for single MSC and MSC array. This confirms the long cycle life of the fabricated MSCs.

The electrochemical impedance spectrum (EIS) was obtained in the frequency range from 500 kHz to 0.1 kHz. Nyquist impedance plots of single MSC and MSC array are shown in Figure 3d. The equivalent series resistance (ESR) was estimated to be 66 and 133 Ω for single MSC and MSC array, respectively. In the low frequency range, the curve shows a vertical shape nearly parallel to the y-axis, which indicates the pure capacitive behavior of the devices.[44,45]

FEM analysis was conducted to estimate the strain distribution on the deformable substrate under uniaxial and biaxial stretching conditions, as shown in Figures 4 and 5, respectively. The deformable substrate was modeled by the quadratic hexahedron element C3D20 in the commercial finite element program, ABAQUS.[32,46−48] A neo-Hookean material models are used for the Ecoflex.

The optical images and FEM result of MSC array integrated on the stretchable substrate subjected to 70% uniaxial strain are shown in Figure 4a. As shown in Figure 4b, the applied strain is defined as $\varepsilon_{uniaxial} = (l' - l)/l$, in which l' and l are the elongation and the initial length of the unit module, respectively. Since the modulus of PET films on the top surface of the substrate and those implanted in the substrate is much higher than that of the substrate, the maximum principal strain of the top PET layer is less than 0.01% where the strain of the substrate between two adjacent top PET layers is up to 300% as shown in Figure 4a and 4c.

To examine the effect of PET interlayer implanted in the substrate, the strain distribution and strain along the x-axis are plotted as shown in Figure 4d. To suppress any excessive deformation of the MSC that must have a detrimental effect on the performance of

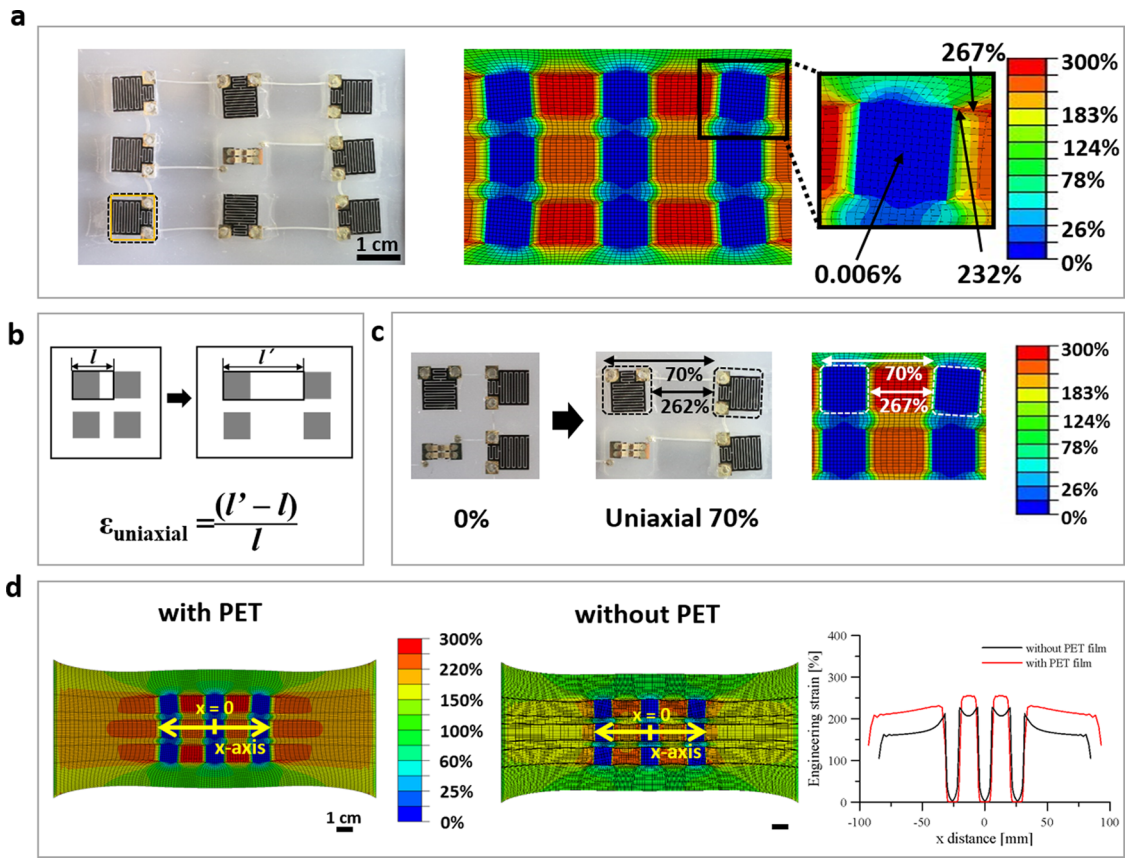

Figure 4. (a) Optical image (left) and FEM analysis (right) of MSC array integrated on the stretchable substrate under 100% uniaxial strains. The yellow and black dashed squares in the optical image indicate the area of MSC and the implanted PET film, respectively. The inset of the strain distribution shows enlarged FEM analysis. (b) Schematic defining applied uniaxial strain ($\varepsilon_{uniaxial}$). (c) Enlarged optical images and FEM analysis of MSC array upon 100% uniaxial stretching. Here, dotted squares indicate the implanted PET films. (d) Comparison of FEM analysis between the substrates with (left) and without (middle) implanted PET, and strain along the *x*-axis under uniaxial strain condition (right).

MSC, the MSC is mounted on the top of the stiff PET layer as shown in Figure 1c. The modulus of the PET is about 2.0 GPa, which is 29 000 times higher than that of the Ecoflex substrate. Thanks to such a high stiffness, the MSC is well protected from the large strain applied to the substrate. However, because of the large difference in the moduli, a significant magnitude of shear stress develops on the interface between the PET layer and the Ecoflex substrate. Note that the membrane deformation of the Ecoflex substrate is suppressed by the PET layer. Because of the shear stress, the strain in the loading direction on the PET layer is minimum at the center and increases gradually to the end of the PET layer; see Figure 4d.

Implantation of the PET interlayer in the middle of the Ecoflex substrate in addition to the PET layer on the top can increase the shear area three times. The increased shear area reduces the membrane strain in the loading direction on the PET layer on the top where the MSC is mounted as shown in Figure 4d (right). According to the current setup, the strain of the top PET layer is almost zero and uniform. The strain of the Ecoflex increases up to 260% with the implanted PET interlayer. This is due to the mechanical compatibility; *i.e.*, the reduced strain of the PET layer must be compensated by the deformation of the Ecoflex substrate. The maximum strain of the Ecoflex with the implanted PET interlayer is 260%, which is 29% of the failure strain limit of the Ecoflex.

The optical images and FEM analysis of biaxially stretched substrate with 50% applied strain are shown in Figure 5a. The applied biaxial strain is defined as shown in Figure 5b. The deformed shape and strain distribution are similar to the case of uniaxial stretching. The top PET layer is almost undeformed as 0.02% and the substrate between two adjacent PET layers is deformed up to 200% as shown in Figure 5a, and 5c. The strain near the corner of the PET layer is much higher than the surrounded region which is marked with gray color in the figure. It seems that the stress increases by the reentrant corner singularity.[49] The strain distribution shown in Figure 5d confirms the beneficial role of the implanted PET interlayers. The MSC array integrated on the stretchable substrate with implanted PET interlayer hardly deforms. Instead, the substrate between two adjacent PET layers deforms more. The strain variation along the *x*-axis is shown in Figure 5d (right). The strain at the

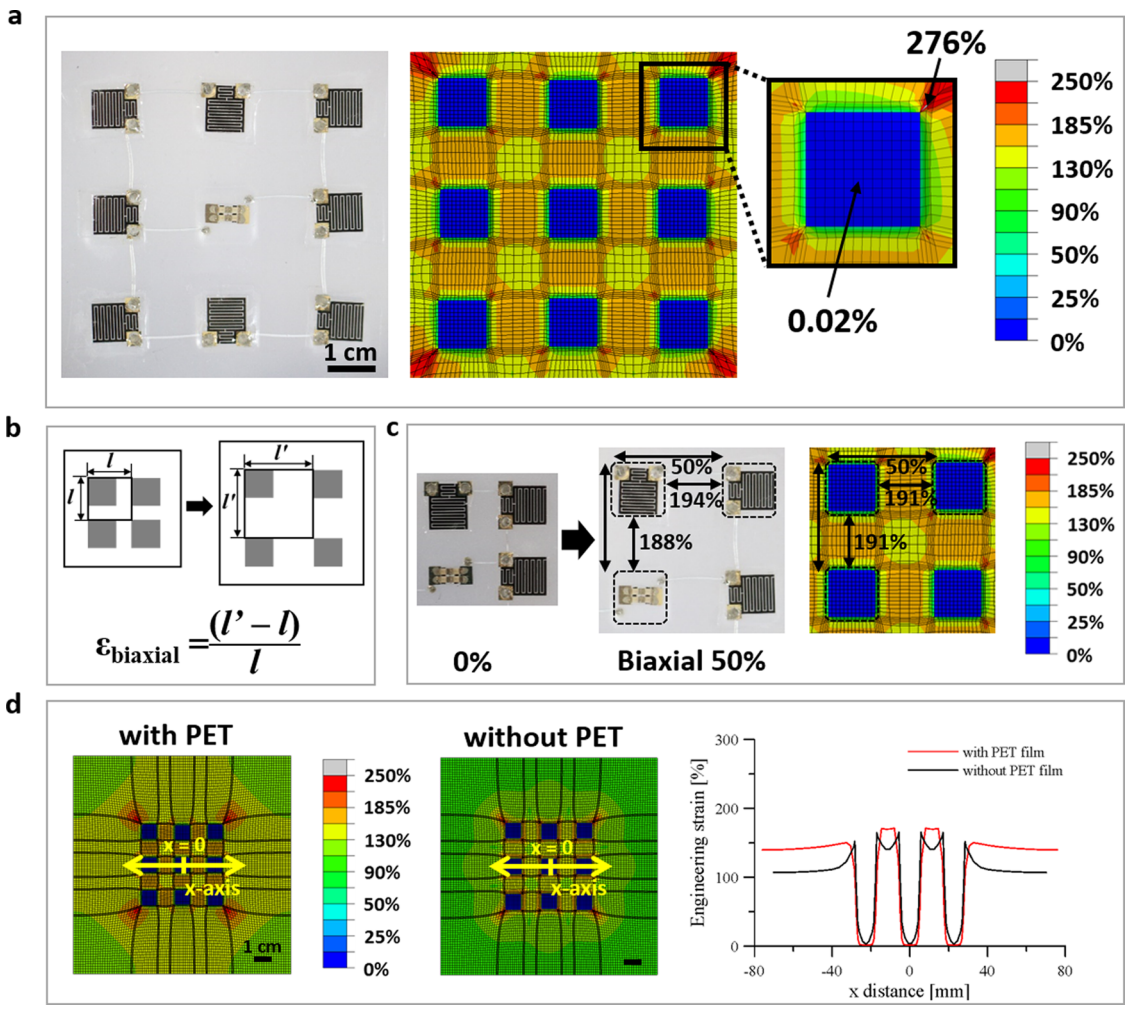

Figure 5. (a) Optical image and FEM analysis of MSC array integrated on the stretchable substrate under 50% biaxial strains. The inset shows enlarged FEM analysis on the single device area. The strain of the gray region exceeded 250% local strain. (b) Schematic defining applied biaxial strain ($\varepsilon_{biaxial}$). (c) Enlarged optical images and FEM analysis of MSC array upon 50% biaxial stretching. Here, the dotted squares indicate the implanted PET films. (d) Comparison of FEM analysis between the substrates with (left) and without (middle) implanted PET, and strain along the *x*-axis under biaxial strain condition (right).

top PET layer is almost zero as expected. The deformation is concentrated in the substrate between two adjacent PET layers as discussed in the previous paragraph.

The electrochemical performance was measured upon uniaxial stretching up to 100%. Galvanostatic charge/discharge and CV curves under uniaxial strain conditions from 0% to 100% are shown in Figure 6a and 6b. Even under severe strain conditions, the device can be operated with no performance degradation due to the strain relieving design of the stretchable substrate. The devices are isolated from strain because it is suppressed on the active device region and concentrated on the trench between adjacent devices. Figure 6c shows that the variation of total capacitance, derived from the CV curves in Figure 6b using eq 1, is within 1%. Specific energy density (E_{cell}) and power density (P_{cell}) were derived from CV curves taken at different scan rates under various strain conditions using the following equations:

$$E = \frac{1}{2} \times C_{sp} \times \frac{(\Delta V)^2}{3600} \quad (3)$$

$$P = \frac{E}{\Delta t} \times 3600 \quad (4)$$

Using the calculated E_{cell} and P_{cell}, a Ragone plot is demonstrated in Figure 6d. No observable change was shown in the graph with variations of strain. The E_{cell} and corresponding P_{cell} values are 25 mWh/cm^3 and 0.74 W/cm^3, respectively. Additionally, the P_{cell} and corresponding E_{cell} values are 31.06 W/cm^3 and 10 mWh/cm^3, respectively. Previously reported works are demonstrated in Supporting Information Figure S6 to compare the energy and power density: lithium thin battery,[50] commercial activated-carbon supercapacitor (AC-SC),[37] Al electrolytic capacitor,[37] laser scribed graphene MSC (LSG-MSC),[51] and graphene-based

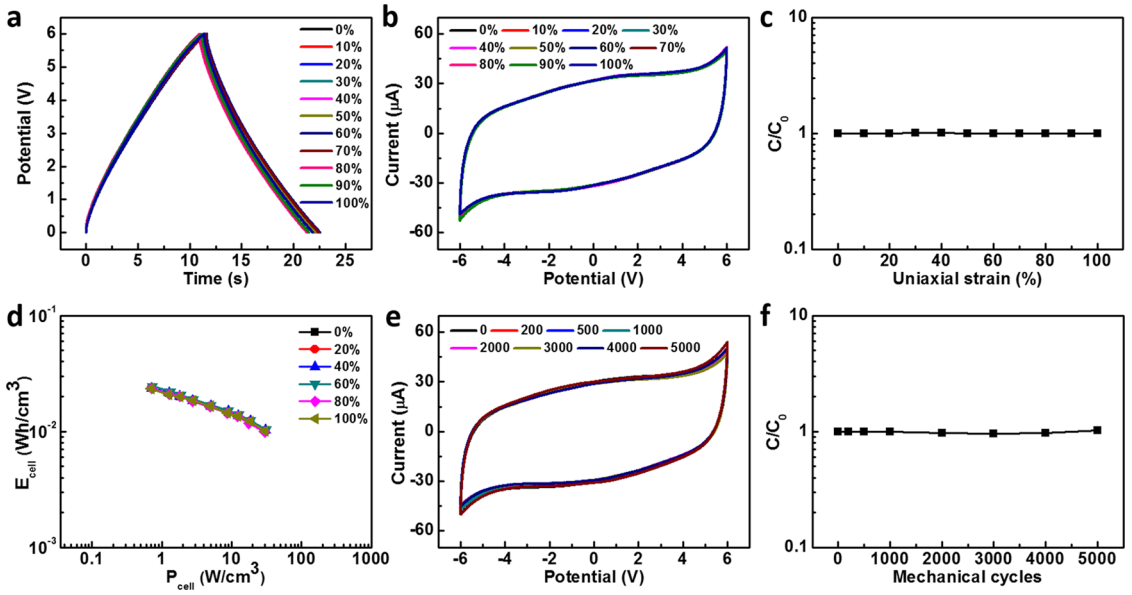

Figure 6. Variations in electrochemical performance upon uniaxial stretching. (a) Galvanostatic charge/discharge curves, (b) CV curves, (c) normalized capacitance *versus* uniaxial strains, and (d) Ragone plots at different scan rates (from 0.1 to 10 V/s) under uniaxial strains from 0 to 100%. (e) CV curves and (f) variations in normalized capacitance upon 5000 repetitions of 70% uniaxial stretching.

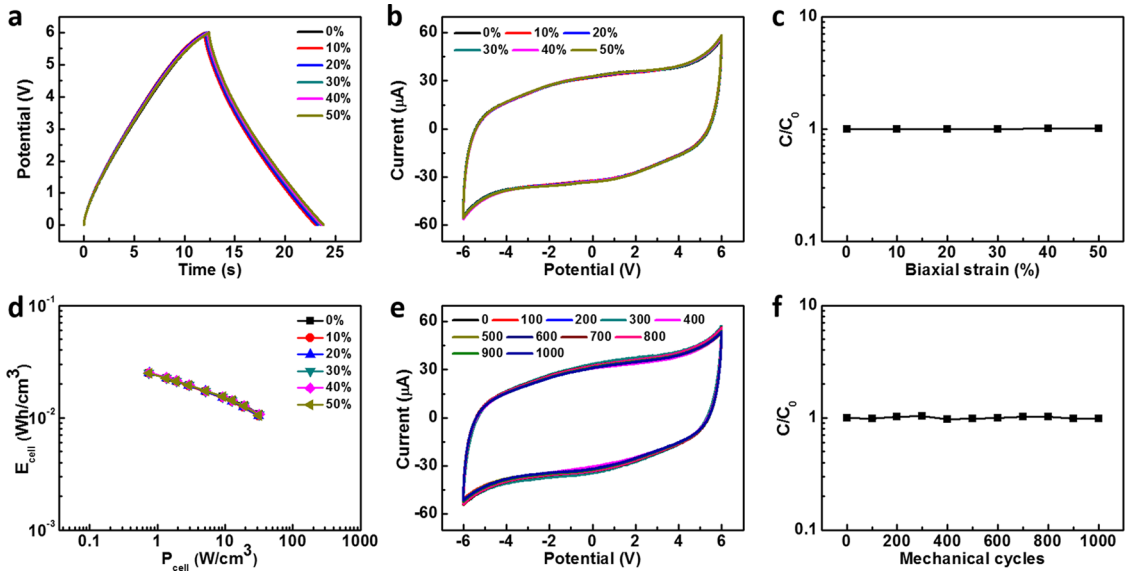

Figure 7. Variations in electrochemical performance upon biaxial stretching. (a) Galvanostatic charge/discharge curves, (b) CV curves, (c) normalized capacitance *versus* biaxial strains, and (d) Ragone plots at different scan rates (from 0.1 to 10 V/s) under biaxial strains from 0 to 50%. (e) CV curves and (f) variations in normalized capacitance upon 1000 repetitions of 30% biaxial stretching.

in-plane MSC (MPG-MSCs).[52] The energy density of our MSC array is 2 orders of magnitude higher than that of the typical AC-SC and even higher than that of a lithium thin battery (<10 mWh/cm^3). The power density of our MSC array is also much higher than that of the conventional AC-SC and comparable to that of an Al electrolytic capacitor and previously reported MSCs.[51,52] High energy and power density were obtained by adopting ionogel electrolyte with high potential window and series connection for the MSC array. The mechanical stability of MSC array was examined by measuring CV curves upon repetitive cycles of 70% uniaxial stretching. The measured CV curves are shown in the Figure 6e. Using eq 1, capacitance variation according to the mechanical cycles is plotted in Figure 6f. Even after 5000 mechanical cycles, the capacitance changed within 4%. As indicated by these results, the fabricated MSC array is very stable to repetitive uniaxial stretching cycles.

Figure 7a and 7b demonstrate the galvanostatic charge/discharge and CV curves under biaxial strain. There was no observable change in the electrochemical

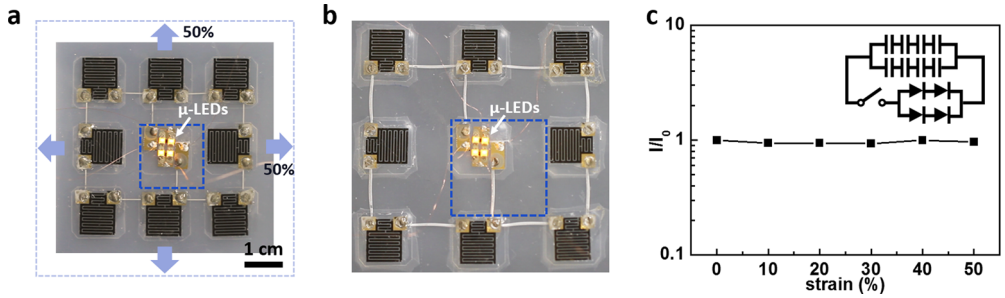

Figure 8. Optical images showing the discharging state of the MSC array lighting μ-LEDs under biaxial strain of (a) 0% and (b) 50%. (c) Variations in brightness upon biaxial stretching up to 50%. The inset is a circuit diagram of 4 $\times$ 2 MSCs connected to the 2 $\times$ 2 μ-LEDs.

performance upon biaxial stretching up to 50%. Total capacitance calculated from the CV curves is shown in Figure 7c. Total capacitance varies within 1% under strain from 0 to 50%. Using the equation mentioned above, E_{cell} and P_{cell} at various scan rates were calculated and plotted in a Ragone plot (Figure 7d). Under biaxial strain up to 50%, no noticeable change was observed. As shown, E_{cell} and the corresponding P_{cell} are 25 mWh/cm^3 and 0.75 W/cm^3, respectively; P_{cell} and the corresponding E_{cell} are 32.18 W/cm^3 and 11 mWh/cm^3, respectively.

Mechanical cycle testing was conducted to examine the durability of the fabricated device against repetitive strains. The CV curves were measured while the device was biaxially stretched 1000 times to 30%. The CV curves shown in Figure 7e were used to calculate the normalized capacitance. As shown in Figure 7f, the capacitance varies within 4% of initial capacitance; additionally, this confirms that the fabricated MSC array can endure repetitive biaxial stretching cycles with no deterioration of the electrochemical performance.

The integrated MSC array was applied to light a μ-LED array because the output voltage was increased considerably *via* the use of ionogel electrolyte with high-potential windows and the integration of multiple MSCs in series. Figure 8a shows the optical image of the fabricated MSC array connected to four μ-LEDs. The turn-on voltage of individual μ-LED is 2 V; thus, the required voltage to turn on the μ-LED array connected in two series and two parallel is expected to be 4 V. The MSC array was charged to 6 V and connected to the μ-LED array to discharge and light the μ-LEDs. Yellow μ-LEDs were lit during discharging of the MSC array under biaxial stretching to a strain of 50%, as shown in Figure 8b. No degradation in the emission characteristics was visible compared to the 0% strain state. The brightness of μ-LEDs according to different strain states is plotted in Figure 8c. The emission performance shows almost no change upon stretching to 50%. The inset represents a circuit diagram of eight MSCs connected in four series and two parallel, and four μ-LEDs connected in two series and two parallel. Consequently, the output voltage of the integrated MSC array is sufficiently high that several μ-LEDs can be operated using the discharging energy of the MSC array; additionally, the MSC array can accommodate biaxial strains to maintain the brightness of μ-LEDs without degradation. This confirms that the strain can be effectively suppressed in the active device area due to the stiff PET films implanted below. Top surface of stiff PET region is hardly strained even when the whole substrate is deformed severely.

CONCLUSION

We report on the fabrication of a biaxially stretchable microsupercapacitor array on a deformable substrate designed to minimize the strain applied to the active region of the device. The deformable substrate is made of soft Ecoflex with locally implanted stiff PET films in which the liquid metal interconnection is embedded. Due to the differences in stiffness between the soft Ecoflex and PET films, local strain is suppressed on the surface area above the PET films. MSCs are fabricated with functionalized MWNT electrodes and patterned high-output-voltage ionogel electrolyte. Individual MSCs are connected into a series and parallel assembly according to the requirements of high output voltage. The MSC array was integrated on the deformable substrate with no degradation of electrochemical performance and was operated stably under up to 50% biaxial and 100% uniaxial strain, according to the FEM analysis results. A μ-LED array was lit by using the high-output voltage of the integrated MSC array. This work demonstrates a high potential of our fabricated MSC array for application as an embedded energy storage device for wearable and bioimplantable devices.

METHODS

Fabrication of Ti/Au Current Collector of MSC. PDMS (Sylgard 184, Dow Corning) is spin-coated onto the Si/SiO_2 substrate at 4000 rpm for 50 s and cured at 65 °C for 1.5 h. PET film (75 μm) is attached on the surface of the PDMS to be used as a substrate for MSC. An interdigitated Ti/Au (5 nm/50 nm)

electrode is fabricated *via* photolithography and e-beam evaporation (KVE-T4065, Korea Vacuum Tech).

Functionalization of MWNTs. To functionalize MWNT with a carboxylic acid group (−COOH), 500 mg of MWNT (Sigma-Aldrich) are refluxed with a solution of 30 mL of H_2SO_4 and 10 mL of HNO_3 at 70 °C for 3 h. After refluxing, 200 mL of DI water is added to the MWNT/acid solution and vacuum filtered through the mixed cellulose ester film (pore size of 0.2 μm, Advantec MFS, Inc.). This fabricated MWNT-COOH film is dispersed in 250 mL of DI water and vacuum filtered; this process is repeated three times to remove the remaining acid. Next, the MWNT-COOH film is dispersed in DI water and placed into a dialysis tube cellulose membrane (MW = 12 K, Sigma-Aldrich) to be dialyzed in a DI water bath with stirring. After dialysis is completed, the MWNT-COOH dispersion is vacuum filtered and dried at room temperature. Then, the fabricated MWNT-COOH film is dispersed in DI water at a concentration of 1 mg/1 mL.

MWNT can be functionalized with an amino functional group ($-NH_2$) by mixing the MWNT dispersion (1 mg/1 mL) with 1-ethyl-3-(3-(dimethylamino)propyl) carbodiimide (EDC, Sigma-Aldrich) and $C_2H_4(NH_2)_2$ (Sigma-Aldrich) and stirring for 5 h. This mixed dispersion is vacuum filtered and redispersed. The dispersion is finally dialyzed by using a dialysis tube.

LbL Assembly of MWNT Film. Functionalized MWNT film can be deposited onto the Ti/Au current collector by alternately dipping the current collector in the prepared MWNT-COOH and MWNT MWNT-NH_2 dispersions for 10 min. The Ti/Au current collector should be rinsed thoroughly with DI water after each dipping process. This unit cycle is repeated 10 times to deposit 10 bilayer functionalized MWNT thin films.

Synthesis and Patterning of Ionogel Electrolyte. The UV-curable ion-gel electrolyte can be synthesized by mixing the ionic liquid, monomer, and UV cross-linking initiator. [EMIM][TFSI] (Sigma-Aldrich), PEGDA (Sigma-Aldrich), and 2-hydroxy-2-methylpropiophenone (HOMPP, Sigma-Aldrich) are mixed at a weight ratio of 88:8:4.[53] The prepared ionogel electrolyte is drop-cast on the MSC electrodes. UV light is irradiated through a shadow mask for 40 s. The UV exposed parts become a thin solid film and the unexposed parts are removed by rinsing with chloroform for 5 s. The remaining parts are rinsed with DI water and dried with N_2 gas.

Fabrication of Liquid Metal Interconnection and Integration of the MSC Array. Galinstan (68.5% Ga, 21.5% In, and 10% Sn; Rotometals) is injected into the microchannels (width: 300 μm; depth: 300 μm) embedded within the substrate. A *via* hole with a diameter of 2 mm is punched on each Au pad of the MSCs. Next, the MSCs are dry-transferred onto the substrate, below which the PET films are implanted, by using a small amount of uncured Ecoflex as adhesive. To electrically connect each MSC to the liquid metal interconnection, Ag NW dispersion (1 wt % diluted in water, diameter: 65 nm, average length: 10 μm; Ditto Technologies) is drop-cast to form an Ag NW contact. The Ag NW percolation electrically connects the individual devices and interconnections, stably sealing the microchannel. Then, uncured PDMS is pasted onto the Ag NW contact for further protection.

Characterization of Stretchable MSC Array. The electrochemical performance of the fabricated MSC array was estimated by measuring CV, galvanostatic charge/discharge curve, and electrochemical impedance spectroscopy using an electrochemical analyzer (Compact Stat, Ivium Technologies). SEM images of the functionalized MWNT film were obtained (Hitachi S-4800).

Conflict of Interest: The authors declare no competing financial interest.

Acknowledgment. This work was supported by the National Research Foundation of Korea (NRF) grant funded by the Korea government (MEST) (Grant No. NRF-2013R1A2A1A01016165). We also thank the KU-KIST Graduate School Program of Korea University, Korea.

Supporting Information Available: Electrical measurement of liquid metal interconnection, SEM image, cross-sectional SEM image of LbL deposited MWNT film, CV curves of eight differently fabricated MSCs *via* LbL assembly at a scan rate of 1 V/s, schematic of MSC array connected 4S + 2P, cross-sectional view of the fabricated deformable substrate, schematic of the fabricated MSC, CV curves of single MSC and MSC array at scan rates from 0.1 to 10 V/s, galvanostatic charge/discharge curves of single MSC and MSC array at current from 6.6 to 19.8 μA, and Ragone plot of out single MSC and MSC array compared with previously reported works. This material is available free of charge *via* the Internet at http://pubs.acs.org.

REFERENCES AND NOTES

1. Kim, D.-H.; Rogers, J. A. Stretchable Electronics: Materials Strategies and Devices. *Adv. Mater.* **2008**, *20*, 4887–4892.
2. Rogers, J. A.; Someya, T.; Huang, Y. Materials and Mechanics for Stretchable Electronics. *Science* **2010**, *327*, 1603–1607.
3. Kim, R.-H.; Bae, M.-H.; Kim, D. G.; Cheng, H.; Kim, B. H.; Kim, D.-H.; Li, M.; Wu, J.; Du, F.; Kim, H.-S.; *et al.* Stretchable, Transparent Graphene Interconnects for Arrays of Microscale Inorganic Light Emitting Diodes on Rubber Substrate. *Nano Lett.* **2011**, *11*, 3881–3886.
4. Sekitani, T.; Nakajima, H.; Maeda, H.; Fukushima, T.; Aida, T.; Hata, K.; Someya, T. Stretchable Active-Matrix Organic Light-Emitting Diode Display Using Printable Elastic Conductors. *Nat. Mater.* **2009**, *8*, 494–499.
5. Cheng, S.; Wu, Z. Microfluidic Stretchable RF Electronics. *Lab Chip* **2010**, *10*, 3227–3234.
6. Lipomi, D. J.; Vosgueritchian, M.; Tee, B. C-K.; Hellstrom, S. L.; Lee, J. A.; Fox, C. H.; Bao, Z. Skin-Like Pressure and Strain Sensors Based on Transparent Elastic Films of Carbon Nanotubes. *Nat. Nanotechnol.* **2011**, *6*, 788–792.
7. Shin, G.; Yoon, C. H.; Bae, M. Y.; Kim, Y. C.; Hong, S. K.; Rogers, J. A.; Ha, J. S. Stretchable Field-Effect-Transistor Array of Suspended SnO_2 Nanowires. *Small* **2011**, *7*, 1181–1185.
8. Kim, D.-H.; Lu, N.; Ma, R.; Kim, Y.-S.; Kim, R.-H.; Wang, S.; Wu, J.; Won, S. M.; Tao, H.; Islam, A.; *et al.* Epidermal Electronics. *Science* **2011**, *333*, 838–843.
9. Meng, Y.; Zhao, Y.; Hu, C.; Cheng, H.; Hu, Y.; Zhang, Z.; Shi, G.; Qu, L. All-Graphene Core-Sheath Microfibers for All-Solid-State, Stretchable Fibriform Supercapacitors and Wearable Electronic Textiles. *Adv. Mater.* **2013**, *25*, 2326–2331.
10. Fu, Y.; Cai, X.; Wu, H.; Lv, Z.; Hou, S.; Peng, M.; Yu, X.; Zou, D. Fiber Supercapacitors Utilizing Pen Ink for Flexible/Wearable Energy Storage. *Adv. Mater.* **2012**, *24*, 5713–5718.
11. Li, L.; Wu, Z.; Yuan, S.; Zhang, X. B. Advances and Challenges for Flexible Energy Storage and Conversion Devices and Systems. *Energy Environ. Sci.* **2014**, *7*, 2101–2122.
12. Yuan, C. Z.; Gao, B.; Shen, L. F.; Yang, S. D.; Hao, L.; Lu, X. J.; Zhang, F.; Zhang, L. J.; Zhang, X. G. Hierarchically Structured Carbon-based Composites: Design, Synthesis and their Application in Electrochemical Capacitor. *Nanoscale* **2011**, *3*, 529–545.
13. Jiang, H.; Lee, P. S.; Li, C. 3D Carbon Based Nanostructures for Advanced Supercapacitors. *Energy Environ. Sci.* **2013**, *6*, 41–53.
14. Choi, B. G.; Hong, J.; Hong, W. H.; Hammond, P. T.; Park, H. Facilitated Ion Transport in All-Solid-State Flexible Supercapacitors. *ACS Nano* **2011**, *5*, 7205–7213.
15. Jung, H. Y.; Karimi, M. B.; Hahm, M. G.; Ajayan, P. M.; Jung, Y. J. Transparent, Flexible Supercapacitors from Nano-engineered Carbon Films. *Sci. Rep.* **2012**, *2*, 773.
16. Zhang, L. L.; Zhao, X. S. Carbon-Based Materials as Supercapacitor Electrodes. *Chem. Soc. Rev.* **2009**, *38*, 2520–2531.
17. Yan, C.; Lee, P. S. Stretchable Energy Storage and Conversion Devices. *Small* **2014**, 10.1002/smll.201302806.
18. Yu, C.; Masarapu, C.; Rong, J.; Wei, B.; Jiang, H. Stretchable Supercapacitors Based on Buckled Single-Walled Carbon Nanotube Macrofilms. *Adv. Mater.* **2009**, *21*, 4793–4797.
19. Xie, Y.; Liu, Y.; Zhao, Y.; Tsang, Y. H.; Lau, S. P.; Huang, H.; Chai, Y. Stretchable All-Solid-State Supercapacitor with Wavy Shaped Polyaniline/Graphene Electrode. *J. Mater. Chem. A* **2014**, *2*, 9142–9149.
20. Kim, D.; Shin, G.; Kang, Y. J.; Kim, W.; Ha, J. S. Fabrication of a Stretchable Solid-State Micro-Supercapacitor Array. *ACS Nano* **2013**, *7*, 7975–7982.
21. Hu, L.; Pasta, M.; Mantia, F. L.; Cui, L.; Jeong, S.; Deshazer, H. D.; Choi, J. W.; Han, S. M.; Cui, Y. Stretchable, Porous, and Conductive Energy Textiles. *Nano Lett.* **2010**, *10*, 708–714.

22. Yue, B.; Wang, C.; Ding, X.; Wallace, G. G. Polypyrrole Coated Nylon Lycra Fabric as Stretchable Electrode for Supercapacitor Applications. *Electrochim. Acta* **2012**, *68*, 18–24.
23. Niu, Z.; Dong, H.; Zhu, B.; Li, J.; Hng, H. H.; Zhou, W.; Chen, X.; Xie, S. Highly Stretchable, Integrated Supercapacitors Based on Single-Walled Carbon Nanotube Films with Continuous Reticulate Architecture. *Adv. Mater.* **2013**, *25*, 1058–1064.
24. Meng, C.; Liu, C.; Chen, L.; Hu, C.; Fan, S. Highly Flexible and All-Solid-State Paperlike Polymer Supercapacitors. *Nano Lett.* **2010**, *10*, 4025–4031.
25. Peng, L.; Peng, X.; Liu, B.; Wu, C.; Xie, Y.; Yu, G. Ultrathin Two-Dimensional MnO_2/Graphene Hybrid Nanostructures for High-Performance, Flexible Planar Supercapacitors. *Nano Lett.* **2013**, *13*, 2151–2157.
26. Niu, Z.; Zhang, L.; Liu, L.; Zhu, B.; Dong, H.; Chen, X. All-Solid-State Flexible Ultrathin Micro-Supercapacitors Based on Graphene. *Adv. Mater.* **2013**, *25*, 4035–4042.
27. Kramer, R. K.; Majidi, C.; Wood, R. J. Masked Deposition of Gallium-Indium Alloys for Liquid-Embedded Elastomer Conductors. *Adv. Funct. Mater.* **2013**, *23*, 5292–5296.
28. Lu, T.; Finkenauer, L.; Wissman, J.; Majidi, C. Rapid Prototyping for Soft-Matter Electronics. *Adv. Funct. Mater.* **2014**, *24*, 3351–3356.
29. Ladd, C.; So, J.-H.; Muth, J.; Dickey, M. D. 3D Printing of Free Standing Liquid Metal Microstructures. *Adv. Mater.* **2013**, *25*, 5081–5085.
30. Tabatabai, A.; Fassler, A.; Usiak, C.; Majidi, C. Liquid-Phase Gallium−Indium Alloy Electronics with Microcontact Printing. *Langmuir* **2013**, *29*, 6194–6200.
31. Boley, J. W.; White, E. L.; Chiu, G. T.-C.; Kramer, R. K. Direct Writing of Gallium-Indium Alloy for Stretchable Electronics. *Adv. Funct. Mater.* **2014**, *24*, 3501–3507.
32. Hong, S. Y.; Yoon, J.; Jin, S. W.; Lim, Y.; Lee, S.-J.; Zi, G.; Ha, J. S. High-Density, Stretchable, All-Solid-State Microsupercapacitor Arrays. *ACS Nano* **2014**, *8*, 8844–8855.
33. Park, Y.-L.; Chen, B.-S.R.; Wood, R. J. Design and Fabrication of Soft Artificial Skin Using Embedded Microchannels and Liquid Conductors. *IEEE Sens. J.* **2012**, *12*, 2711–2718.
34. Nakahara, R.; Uno, M.; Uemura, T.; Takimiya, K.; Takeya, J. Flexible Three-Dimensional Organic Field-Effect Transistors Fabricated by an Imprinting Technique. *Adv. Mater.* **2012**, *24*, 5212–5216.
35. Dickey, M. D.; Chiechi, R. C.; Larson, R. J.; Weiss, E. A.; Weitz, D. A.; Whitesides, G. M. Eutectic Gallium-Indium (EGaIn): A Liquid Metal Alloy for the Formation of Stable Structures in Microchannels at Room Temperature. *Adv. Funct. Mater.* **2008**, *18*, 1097–1104.
36. Cheng, S.; Wu, Z. Microfluidic Electronics. *Lab Chip* **2012**, *12*, 2782–2791.
37. El-Kady, M. F.; Strong, V.; Dubin, S.; Kaner, R. B. Laser Scribing of High-Performance and Flexible Graphene-Based Electrochemical Capacitors. *Science* **2012**, *335*, 1326–1330.
38. Fan, Z.; Yan, J.; Wei, T.; Zhi, L.; Ning, G.; Li, T.; Wei, F. Asymmetric Supercapacitors Based on Graphene/MnO_2 and Activated Carbon Nanofiber Electrodes with High Power and Energy Density. *Adv. Funct. Mater.* **2011**, *21*, 2366–2375.
39. Yun, J.; Kim, D.; Lee, G.; Ha, J. S. All-Solid-State Flexible Micro-Supercapacitor Arrays with Patterned Graphene/MWNT Electrodes. *Carbon* **2014**, *79*, 156–164.
40. Niu, Z.; Zhou, W.; Chen, J.; Feng, G.; Li, H.; Ma, W.; Li, J.; Dong, H.; Ren, Y.; Zhao, D.; *et al.* Compact-Designed Supercapacitors Using Free-Standing Single-Walled Carbon Nanotube Films. *Energy Environ. Sci.* **2011**, *4*, 1440–1446.
41. Shah, R.; Zhang, X.; Talapatra, S. Electrochemical Double Layer Capacitor Electrodes Using Aligned Carbon Nanotubes Grown Directly on Metals. *Nanotechnology* **2009**, *20*, 395202.
42. Zhu, Y.; Murali, S.; Stoller, M. D.; Ganesh, K. J.; Cai, W.; Ferreira, P. J.; Pirkle, A.; Wallace, R. M.; Cychosz, K. A.; Thommes, M.; *et al.* Carbon-Based Supercapacitors Produced by Activation of Graphene. *Science* **2011**, *332*, 1537–1541.
43. Yang, X.; Zhang, L.; Zhang, F.; Zhang, T.; Huang, Y.; Chen, Y. A High-Performance All-Solid-State Supercapacitor with Graphene-Doped Carbon Material Electrodes and a Graphene Oxide-Doped Ion Gel Electrolyte. *Carbon* **2014**, *72*, 381–386.
44. Liu, C.; Yu, Z.; Neff, D.; Zhamu, A.; Jang, B. Z. Graphene-Based Supercapacitor with an Ultrahigh Energy Density. *Nano Lett.* **2010**, *10*, 4863–4868.
45. Gao, K.; Shao, Z.; Li, J.; Wang, X.; Peng, X.; Wang, W.; Wang, F. Cellulose Nanofiber-Graphene All Solid-State Flexible Supercapacitors. *J. Mater. Chem. A* **2013**, *1*, 63–67.
46. *ABAQUS Version 6.10 User's Manual*; Hibbitt, Karlson & Sorensen, Inc.: Providence, RI, 2012.
47. Shin, G.; Bae, M. Y.; Lee, H. J.; Hong, S. K.; Yoon, C. H.; Zi, G.; Rogers, J. A.; Ha, J. S. SnO_2 Nanowire Logic Devices on Deformable Non-Planar Substrates. *ACS Nano* **2011**, *5* (12), 10009.
48. Yoon, J.; Hong, S. Y.; Lim, Y.; Lee, S.-J.; Zi, G.; Ha, J. S. Design and Fabrication of Novel Stretchable Device Arrays on a Deformable Polymer Substrate with Embedded Liquid Metal Interconnections. *Adv. Mater.* **2014**, 10.1002/adma.201402588.
49. Bažant, Z. P.; Yu, Q. Size Effect on Strength of Quasibrittle Structures with Reentrant Corners Symmetrically Loaded in Tension. *J. Eng. Mech. Div., Am. Soc. Civ. Eng.* **2006**, *132* (11), 1168.
50. Pech, D.; Brunet, M.; Durou, H.; Huang, P. H.; Mochalin, V.; Gogotsi, Y.; Taberna, P. L.; Simon, P. Ultrahigh-Power Micrometre-Sized Supercapacitors Based on Onion-Like Carbon. *Nat. Nanotechnol.* **2010**, *5*, 651–654.
51. El-Kady, M. F.; Kaner, R. B. Scalable Fabrication of High-Power Graphene Micro-Supercapacitors for Flexible and On-Chip Energy Storage. *Nat. Commun.* **2013**, *4*, 1475.
52. Wu, Z.-S.; Parvez, K.; Feng, X.; Mullen, K. Graphene-Based In-Plane Micro-Supercapacitors with High Power and Energy Densities. *Nat. Commun.* **2013**, *4*, 2487.
53. Lee, S. W.; Lee, H. J.; Choi, J. H.; Koh, W. G.; Myoung, J. M.; Hur, J. H.; Park, J. J.; Cho, J. H.; Jeong, U. Periodic Array of Polyelectrolyte-Gated Organic Transistors from Electrospun Poly(3-hexylthiophene) Nanofibers. *Nano Lett.* **2010**, *10*, 347–351.